

Entanglement Spectroscopy using Quantum Monte Carlo

Chia-Min Chung,^{1,2,*} Lars Bonnes,^{1,†} Pochung Chen,^{2,3} and Andreas M. Läuchli¹

¹*Institute for Theoretical Physics, University of Innsbruck, A-6020 Innsbruck, Austria*

²*Department of Physics, National Tsing Hua University, Hsinchu 30013, Taiwan*

³*Frontier Research Center on Fundamental and Applied Sciences of Matters, National Tsing Hua University, Hsinchu 30013, Taiwan*

(Dated: July 25, 2018)

We present a numerical scheme to reconstruct a subset of the entanglement spectrum of quantum many body systems using quantum Monte Carlo. The approach builds on the replica trick to evaluate particle number resolved traces of the first n of powers of a reduced density matrix. From this information we reconstruct n entanglement spectrum levels using a polynomial root solver. We illustrate the power and limitations of the method by an application to the extended Bose-Hubbard model in one dimension where we are able to resolve the quasi-degeneracy of the entanglement spectrum in the Haldane-Insulator phase. In general the method is able to reconstruct the largest few eigenvalues in each symmetry sector and typically performs better when the eigenvalues are not too different.

I. INTRODUCTION

The field of quantum many body systems has been boosted tremendously by the investigation of quantum information motivated quantities such as von Neumann or Renyi entanglement entropies applied to strongly correlated quantum matter¹. Important achievements are the discovery of area laws controlling the entanglement properties of ground states of local gapped Hamiltonians², that entanglement entropies encode topological properties of matter³⁻⁶, or that the logarithmic corrections of the area law in one-dimensional critical systems are governed by the central charge of the underlying conformal field theory (CFT)⁷⁻⁹.

More recently the entanglement spectrum - i.e. the negative logarithm of the eigenvalues of a reduced density matrix - has been proposed as a novel tool to obtain insightful information beyond the information content of individual entanglement entropies¹⁰. More specifically let us consider a bipartition of a system into two complementary parts A and B and the corresponding Schmidt decomposition of a wave function $|\psi\rangle$:

$$|\psi\rangle = \sum_i e^{-\xi_i/2} |\psi_i^A\rangle \otimes |\psi_i^B\rangle, \quad (1)$$

where $|\psi_i^A\rangle$ and $|\psi_i^B\rangle$ are orthonormal vectors in subsystems A and B respectively, and ξ_i are the so called entanglement spectrum levels, related to the eigenvalues λ_i of the corresponding reduced density matrix through the relation $\xi_i = -\ln \lambda_i$. It was shown in Ref. 10 that for fractional quantum Hall states the entanglement spectrum ξ_i arranges in close analogy to the energy spectrum of a physical edge. This observation sparked a lot of activity exploring the physical information contained in the entanglement spectrum e.g. in topological quantum matter¹⁰⁻²⁶, in continuous symmetry breaking states^{27,28} or in one-dimensional critical systems described by a CFT²⁹⁻³².

So far numerical entanglement spectra have been obtained mainly using wave function based numerical approaches such as Exact Diagonalization^{10,12-15}, Density Matrix renormalization Group (DMRG)^{16,31-36} or Tensor Network states³⁷. Mo-

tivated by recent advances in measuring Renyi entropies in Quantum Monte Carlo methods (QMC)³⁸⁻⁴⁰ we want to explore in this paper to what extent current Quantum Monte Carlo methods are suitable to reconstruct entanglement spectra.

The basic idea is to measure the trace of the first n powers of a reduced density matrix using a replica approach, and then to infer n eigenvalues of the reduced density matrices based on the measured moments. This problem is a particular instance of the (truncated) Hausdorff problem^{41,42} and known to be an ill-conditioned problem, similar to the analytic continuation problem arising in the Monte Carlo evaluation of spectral functions. An additional complication is the presence of statistical uncertainties of the Renyi entropies similar to the situation of a statistical Hausdorff problem considered in Ref. 43.

With these limitations in mind it is our goal to explore how far one can go with current technologies. While the full reconstruction of the entanglement spectrum is clearly out of reach, a particle number resolved measurement technique allows us to track roughly the lowest few entanglement spectra levels per sector with reasonable effort, provided the eigenvalues are of similar magnitude.

We illustrate the approach by simulating the one-dimensional extended Bose-Hubbard model focusing on the Mott insulator and the Haldane insulator. We demonstrate that our QMC approach is able to detect the quasi-degeneracy of the entanglement spectrum in the Haldane insulator versus the non-degeneracy in the Mott insulator.

II. METHOD

A. QMC Implementation.

The n th Renyi entropy, $S_A^{(n)}$, can be accessed in (quantum) Monte Carlo using the replica trick³⁸ that links the n th moment of the reduced density matrix to a ratio of two partition

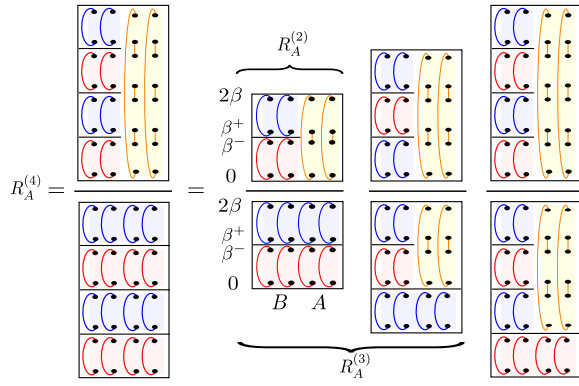


Figure 1. (Color online) Illustration of the world line connectivity required for the calculation of $R_A^{(4)}$. The right hand side illustrates the *imaginary time increment trick* used to estimate $R_A^{(n)}$.

functions,

$$R_A^{(n)} \equiv \text{Tr} \rho_A^n = \frac{Z_A^{(n)}}{Z^n}, \quad (2)$$

and $S_A^{(n)} = 1/(1-n) \log R_A^{(n)}$. $Z = \text{Tr} \exp(-\beta H)$ denotes the usual partition function for a system at temperature $T = 1/\beta$ and $Z_A^{(n)}$ is the partition function living on a n -sheeted Riemann surface of temporal extent $n\beta$ with $n-1$ equal-time branch-cuts at times $m\beta$ ($m = 1, \dots, n-1$) along the extent of subsystem A . Here we use a continuous time worm algorithm⁴⁴⁻⁴⁶ that operates in the path integral representation of the partition functions and allows for an efficient sampling of $R_A^{(n)}$ when the normal world-line update is supplemented with a global update scheme devised in Ref. 40. Starting from Z^n , the global update tries to connect the world lines along the branch cuts within A . If the world lines at $m\beta^-$ can be connected to $m\beta^+$ (note the periodicity in imaginary time), the world line sheets are transformed to this non-trivial geometry $Z_A^{(n)}$, as illustrated in Fig. 1. An inverse move tries to recut the world lines at all $m\beta^-$ and $m\beta^+$. $R_A^{(n)}$ is estimated by simply counting how often the system is in one or the other world line configuration.

As A grows the transition probability in the global update decreases rapidly and the simulation becomes rather inefficient. By expanding Eq. (2) as $[Z_{A_1}^{(n)}/Z^{(n)}][Z_{A_2}^{(n)}/Z_{A_1}^{(n)}] \dots [Z_{A_k}^{(n)}/Z_{A_{k-1}}^{(n)}]$ with $A_1 \subset A_2 \subset \dots \subset A_k \subset \bar{A}$, large subsystem sizes can be accessed by successively growing the subsystem and evaluating each partition function ratio in square brackets separately³⁹.

Accessing higher Renyi entropies poses a similar challenge since the number of branch cuts increases. To cure this inefficiency, we conceive an *imaginary time increment trick* by realizing that the partition function ratio can be rewritten as

$$R_A^{(n)} = \frac{Z_A^{(n-1)}}{Z^{n-1}} \frac{Z_A^{(n)}}{Z_{A_1}^{(n-1)}} = R_A^{(n-1)} \frac{Z_A^{(n)}}{Z_{A_1}^{(n-1)}}. \quad (3)$$

Thus, the n th Renyi entropy requires the calculation of

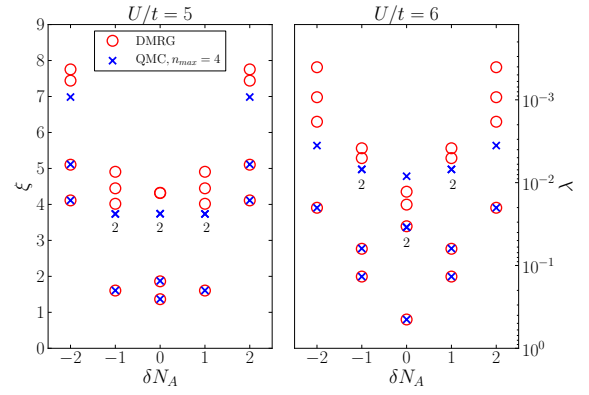


Figure 2. (Color online) Lower part of the particle number resolved entanglement spectrum of a block of length $L_A = 24$ in a periodic chain with $L = 48$ of an extended Bose-Hubbard model at unit filling with $V/t = 3.3$ and $U/t = 5$ (HI, left panel) and $U/t = 6$ (MI, right panel) obtained using $n_{\max} = 4$. An (artificial) degeneracy is indicated by numbers below the data points. Only the lowest four DMRG levels per sector are shown.

$R_A^{(n-1)}$ as well as the evaluation of a partition function ratio between two geometries with a *single* branch cut, as illustrated in Fig. 1. This improved scheme allows us to access Renyi entropies as high as $n = 4$ and can readily be generalized to different implementations. Although it is possible to access also higher Renyi entropies efficiently with this update scheme we restricted ourselves to the calculation of up to the fourth moment since including higher moments will not improve the reconstruction of the entanglement spectrum given the current accuracy of our data as it will be detailed in the following section.

B. Reconstructing the Entanglement Spectrum.

The knowledge of all integer Renyi entropies in principle provides all the information required to extract the entanglement spectrum²⁹ by, for instance, solving a large system of coupled non-linear equations. We explored several entanglement spectrum reconstruction approaches including an optimization techniques over the n eigenvalues. Since this operation has to be performed many times in the binning analysis of the Monte Carlo time series, we chose to rely on the recent work by Song *et al.*⁴⁷, which presented a nice way to relate the $R_A^{(n)}$ quantities to the characteristic polynomial of ρ_A .⁴⁸ In our setup we can only get accurate data up to certain n , so we simply approximate the full characteristic polynomial by an order n truncation. Finding the roots of a polynomial with noisy coefficients can, in general, be challenging (see e.g. Ref. 49), for example the roots can sometimes shift away from the real axis and cluster in pairs, thereby acquiring a small imaginary part that will be omitted.⁵⁰ This does not, however, affect the normalization condition $\sum_i \lambda_i = 1$ since the imaginary parts cancel.

The main difficulty in reconstructing the spectrum of the reduced density matrix is that the eigenvalues λ can extend

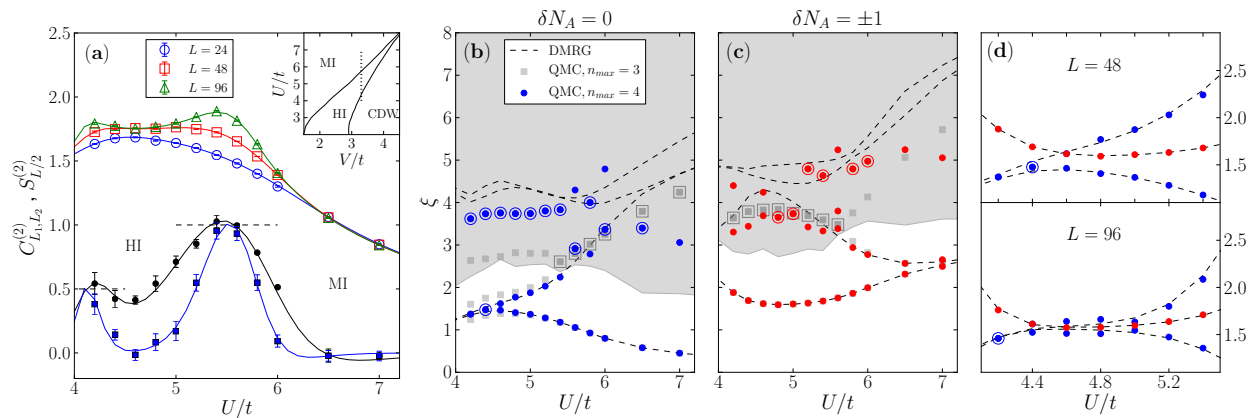


Figure 3. (Color online) (a) Renyi entropies $S_{L/2}^{(2)}$ (open symbols) and the central charge estimator $C_{L_1, L_2}^{(2)}$ for $(L_1, L_2) = (24, 48)$ (filled black dots) and $(48, 96)$ (filled blue square) as a function of U/t for $V/t = 3.3$. The continuous lines denote reference DMRG results. The inset shows part of phase diagram from Ref. 34, where the dotted line indicates the parameter region we focus on. (b),(c) The lower part of ES on $\delta N_A = 0$ and ± 1 as a function of U , gotten by $n_{\max} = 3$ and $n_{\max} = 4$. The open symbols indicate the artificial two-fold degenerate points. The gray shaded area is the regime $\xi > -1/4 \log \delta R_A^{(4)}$ where the ES cannot be resolved accurately. (d) The panel displays lowest two entanglement levels for $\delta N_A = 0$ (blue dots) and $\delta N_A = \pm 1$ (red dots) in the HI for $L = 48$ (from panels (b) and (c)) and $L = 96$ showing the closing of the gap in the entanglement spectrum with increasing system size. The dashed lines in panels (b) to (d) denote the reference DMRG data.

over several orders of magnitude. Higher moments, on the other hand, are dominated by the largest eigenvalue λ_1 , i.e. $R_A^{(n)} = \lambda_1^n (1 + [\lambda_2/\lambda_1]^n + \dots)$, providing a threshold for the resolvable eigenvalues given an error on $R_A^{(n)}$.

An improvement of the reconstruction procedure is to take advantage of the block structure of the density matrix that stems from particle number conservation (or any other quantum numbers that are easily accessible in QMC). To be more specific, we calculate the moments of ρ_A in each particle number sector labelled by $\delta N_A = N_A - \bar{N}_A$ (N_A is the number of particles in block A and \bar{N}_A is the average particle number) separately by binning the measurements into the respective sectors. We combine the data for symmetric blocks with δN_A and $-\delta N_A$ to improve the accuracy of our data.⁵¹

The power of our approach is illustrated in Fig. 2, where we show entanglement spectra for two different parameter sets in a one-dimensional extended Bose Hubbard model. The model as well as the physics of the spectra will be discussed in Sec. III below. Here we just want to highlight the good agreement between the QMC reconstruction of the lowest entanglement spectrum level in each sector (corresponding to the largest eigenvalues λ) and the reference DMRG results. Furthermore also the second entanglement spectrum level in each sector is rather accurate, provided the ξ values are not separated by a large gap from the first level in the same sector.

III. NUMERICAL RESULTS

For a more thorough application we now turn to the extended Bose-Hubbard model here given in terms of standard

bosonic operators as

$$H = -t \sum_i (b_i^\dagger b_{i+1} + \text{h.c.}) + \frac{U}{2} \sum_i n_i (n_i - 1) + V \sum_i n_i n_{i+1}. \quad (4)$$

Recent analytical^{52,53} and numerical^{34,54-56} studies revealed that its phase diagram features a topologically non-trivial Haldane insulating (HI) phase besides more conventional phases such as a Mott insulator (MI) and a charge density wave phase (CDW). The HI is closely linked to the Haldane phase in spin $S = 1$ chains that does not break a local symmetry but has non-local string order and a characteristic degeneracy of the entanglement spectrum protected by a set of symmetries^{16,57}.

We restrict ourselves to the case of unit filling and periodic boundary conditions (PBC) and sketch the phase diagram, obtained from Ref. 55, in the inset of Fig. 3(a). The simulations are performed along the line $V/t = 3.3$ where the system can be tuned from the CDW at lower U to the HI at $U/t \approx 4.15$. Upon further increasing the on-site interaction, one eventually enters the MI at $U/t \approx 5.55$.

A. Locating the Phase Transitions

As a preparatory step we investigate the behavior of the second Renyi entropy of a half system block $L_A = L/2$ across the two phase transitions. In a gapped phase the entropy of a block saturates as a function of the block size by virtue of the strict area law. At a quantum critical point with conformal symmetry however, the entanglement entropies exhibit a logarithmic correction, whose coefficient is directly related to the

central charge c :

$$S_{l'_A}^{(n)}(U_c) = \frac{c}{6} \left(1 + \frac{1}{n}\right) \log l'_A + c'_n, \quad (5)$$

where l'_A is the chord length of block A and c'_n is a non-universal constant. When considering the entropy increment upon increasing the system and block size⁵⁸:

$$C_{L_1, L_2}^{(2)} = \frac{4}{\log L_2/L_1} \left[S_{L_2/2}^{(2)} - S_{L_1/2}^{(2)} \right], \quad (6)$$

this quantity displays a peak at the location of the quantum phase transition and its peak value corresponds to the central charge of the transition. In the gapped phase $C_{L_1, L_2}^{(2)}$ tends to zero with increasing system sizes. In Fig. 3(a) we find two distinct peaks with $c = 1/2$ (CDW-HI) and $c = 1$ (HI-MI) in accordance with the expected presence of an Ising and a Gaussian critical point respectively⁵⁹. Furthermore our QMC data – also for higher Renyi entropies (not shown) – agrees perfectly with the reference DMRG results.

B. Entanglement Reconstruction

We now turn towards the analysis of the entanglement spectrum as a function of U/t for fixed $V/t = 3.3$, focussing on the MI and HI phases. In insightful papers Pollmann *et al.*^{16,57} realized that the HI phase can be characterized by a particular degeneracy structure of the entire entanglement spectrum. In the PBC setup we consider, there are two distinct boundaries separating the two parts of the system and the degeneracy of the lowest lying multiplet is four in this case, with a quantum number structure as shown in the left panel of Fig. 2, i.e. two levels at $\delta N_A = 0$ and one level each at $\delta N_A = \pm 1$.

In Fig. 3(b) and (c) we now display the U/t dependence of the QMC reconstructed ES based on the method outlined in Sec. II B. The gray squares denote data reconstructed using $n_{\max} = 3$, whereas the colored dots correspond to $n_{\max} = 4$. In panel Fig. 3(d) we display the lowest two levels for $\delta N_A = 0$ and $\delta N_A = \pm 1$ for $L = 48$ and 96 in the HI. One can clearly see that the lowest four levels become closer for increasing system size, eventually leading to the four-fold degeneracy in the thermodynamic limit. In fact, the QMC calculations nicely capture this feature and agree with the DMRG results.

Taking either three or four moments of the density matrix, the lowest two levels of the entanglement spectrum can be captured quite well. Although the $n_{\max} = 4$ data for the third level in the $\delta N_A = 0$ sector agrees with the DMRG results qualitatively, the quantitative agreement is not as good as for the lower levels. This effect is readily understood as a small and finite number of entanglement levels will necessarily lead to a deformation of the spectrum – some of the ξ s are typically shifted downwards because the complete trace has to be incorporated in very few levels.

A second observation is that the entanglement gap in the respective particle number sectors has a substantial influence

on the quality of the obtained spectrum. The separation of the ξ values for large U increases the domination of the first level and hence requires a much better resolution as compared to the Haldane phase where the lowest two levels are almost degenerate.

We find that we can actually resolve entanglement levels only below a threshold $\xi \lesssim -1/n \log[\delta R_A^{(n_{\max})}]$ given by the error on the highest moment. This threshold, that is also shown in Fig. 3, stems from the observation that the overall precision of the moments has to be comparable or better than the summands one tries to resolve and also incorporates the fact that smaller eigenvalues of the density matrix are suppressed exponentially, i.e. like $(\lambda_j/\lambda_1)^n$, for increasing n .⁶⁰ Above the error threshold the spectrum easily acquires false degeneracies, as discussed previously, or some of the reconstructed eigenvalues can become purely imaginary and are thus omitted.

IV. SUMMARY AND DISCUSSION

In this paper we have presented an approach to reconstruct the entanglement spectrum of quantum many body systems by measuring particle number resolved higher moments of reduced density matrices in QMC. To effectively calculate larger n Renyi entropies, an enhanced increment scheme is presented that greatly improves the global topology updates of the world lines. We are in fact able to recover the low lying degenerate levels in the HI insulator and show that this degeneracy does not persist in the MI phase where, however, our method fails to quantitatively capture the higher-lying part of the spectrum of the MI because of the large separation of levels.

Our approach is not only limited to the QMC methods described in this paper. Similar procedures can potentially be applied to Variational Monte Carlo (VMC) evaluation of trial wavefunctions, going beyond the 2nd Renyi entropy calculations performed so far^{61–64}, and thus potentially access a few of the largest eigenvalues of the reduced density matrices.

Another interesting aspect is that using the protocol put forward in Ref. 65 it seems possible to both obtain higher $R^{(n)}$ as well as particle number resolved traces $R^{(n)}[\delta N_A]$, so that a partial reconstruction of the entanglement spectrum in experiments on large bosonic systems might become possible in the future.

ACKNOWLEDGMENTS

We acknowledge support by the Austrian Science Fund (FWF) through the SFB FoQuS (FWF Project No. F4018-N23). We acknowledge financial support and allocation of CPU time from NSC and NCTS Taiwan. This work was supported by the Austrian Ministry of Science BMWF as part of the UniInfrastrukturprogramm of the Forschungsplattform Scientific Computing at LFU Innsbruck.

- * chiaminchung@gmail.com
† lars.bonnes@uibk.ac.at
- ¹ L. Amico, R. Fazio, A. Osterloh, and V. Vedral, *Rev. Mod. Phys.* **80**, 517 (2008).
 - ² J. Eisert, M. Cramer, and M. B. Plenio, *Rev. Mod. Phys.* **82**, 277 (2010).
 - ³ A. Kitaev and J. Preskill, *Phys. Rev. Lett.* **96**, 110404 (2006).
 - ⁴ M. Levin and X.-G. Wen, *Phys. Rev. Lett.* **96**, 110405 (2006).
 - ⁵ S. Isakov, M. Hastings, and R. Melko, *Nat. Phys.* **7**, 772 (2011).
 - ⁶ H.-C. Jiang, Z. Wang, and L. Balents, *Nat. Phys.* **8**, 902 (2012).
 - ⁷ C. Holzhey, F. Larsen, and F. Wilczek, *Nucl. Phys. B* **424**, 443 (1994).
 - ⁸ G. Vidal, J. Latorre, E. Rico, and A. Kitaev, *Phys. Rev. Lett.* **90**, 227902 (2003).
 - ⁹ P. Calabrese and J. Cardy, *J. Stat. Mech.*, P06002 (2004).
 - ¹⁰ H. Li and F. Haldane, *Phys. Rev. Lett.* **101**, 010504 (2008).
 - ¹¹ N. Bray-Ali, L. Ding, and S. Haas, *Phys. Rev. B* **80**, 180504 (2009).
 - ¹² N. Regnault, B. A. Bernevig, and F. D. M. Haldane, *Phys. Rev. Lett.* **103**, 016801 (2009).
 - ¹³ A. M. Läuchli, E. J. Bergholtz, J. Suorsa, and M. Haque, *Phys. Rev. Lett.* **104**, 156404 (2010).
 - ¹⁴ R. Thomale, A. Sterdyniak, N. Regnault, and B. A. Bernevig, *Phys. Rev. Lett.* **104**, 180502 (2010).
 - ¹⁵ R. Thomale, D. P. Arovas, and B. A. Bernevig, *Phys. Rev. Lett.* **105**, 116805 (2010).
 - ¹⁶ F. Pollmann, A. M. Turner, E. Berg, and M. Oshikawa, *Phys. Rev. B* **81**, 064439 (2010).
 - ¹⁷ A. M. Turner, Y. Zhang, and A. Vishwanath, *Phys. Rev. B* **82**, 241102 (2010).
 - ¹⁸ M. Kargarian and G. A. Fiete, *Phys. Rev. B* **82**, 085106 (2010).
 - ¹⁹ E. Prodan, T. L. Hughes, and B. A. Bernevig, *Phys. Rev. Lett.* **105**, 115501 (2010).
 - ²⁰ L. Fidkowski, *Phys. Rev. Lett.* **104**, 130502 (2010).
 - ²¹ Z. Papić, B. A. Bernevig, and N. Regnault, *Phys. Rev. Lett.* **106**, 056801 (2011).
 - ²² J. Dubail and N. Read, *Phys. Rev. Lett.* **107**, 157001 (2011).
 - ²³ T. L. Hughes, E. Prodan, and B. A. Bernevig, *Phys. Rev. B* **83**, 245132 (2011).
 - ²⁴ L. Fidkowski, T. S. Jackson, and I. Klich, *Phys. Rev. Lett.* **107**, 036601 (2011).
 - ²⁵ X.-L. Qi, H. Katsura, and A. W. W. Ludwig, *Phys. Rev. Lett.* **108**, 196402 (2012).
 - ²⁶ A. M. Turner, Y. Zhang, R. S. K. Mong, and A. Vishwanath, *Phys. Rev. B* **85**, 165120 (2012).
 - ²⁷ M. A. Metlitski and T. Grover, (2011), [arXiv:1112.5166](https://arxiv.org/abs/1112.5166) (unpublished).
 - ²⁸ V. Alba, M. Haque, and A. M. Läuchli, (2012), [arXiv:1212.5634](https://arxiv.org/abs/1212.5634) (unpublished).
 - ²⁹ P. Calabrese and A. Lefèvre, *Phys. Rev. A* **78**, 032329 (2008).
 - ³⁰ F. Pollmann, S. Mukerjee, A. M. Turner, and J. E. Moore, *Phys. Rev. Lett.* **102**, 255701 (2009).
 - ³¹ G. De Chiara, L. Lepori, M. Lewenstein, and A. Sanpera, *Phys. Rev. Lett.* **109**, 237208 (2012).
 - ³² A. Läuchli, (2013), [arXiv:1303.0741](https://arxiv.org/abs/1303.0741) (unpublished).
 - ³³ K. Okunishi, Y. Hieida, and Y. Akutsu, *Phys. Rev. E* **59**, R6227 (1999).
 - ³⁴ X. Deng and L. Santos, *Phys. Rev. B* **84**, 085138 (2011).
 - ³⁵ X. Deng, R. Citro, E. Orignac, A. Minguzzi, and L. Santos, (2013), [arXiv:1302.0528](https://arxiv.org/abs/1302.0528) (unpublished).
 - ³⁶ H.-C. Jiang, S. Rachel, Z.-Y. Weng, S.-C. Zhang, and Z. Wang, *Phys. Rev. B* **82**, 220403 (2010).
 - ³⁷ J. I. Cirac, D. Poilblanc, N. Schuch, and F. Verstraete, *Phys. Rev. B* **83**, 245134 (2011).
 - ³⁸ R. G. Melko, A. B. Kallin, and M. B. Hastings, *Phys. Rev. B* **82**, 100409 (2010).
 - ³⁹ M. B. Hastings, I. González, A. B. Kallin, and R. G. Melko, *Phys. Rev. Lett.* **104**, 157201 (2010).
 - ⁴⁰ S. Humeniuk and T. Roscilde, *Phys. Rev. B* **86**, 235116 (2012).
 - ⁴¹ F. Hausdorff, *Mathematische Zeitschrift* **9**, 74 (1921).
 - ⁴² J. A. Shohat and J. D. Tamarkin, *The Problem of Moments* (Am. Math. Soc., New York, 1943).
 - ⁴³ T. M. P. Ngoc, *Inv. Prob.* **24**, 045018 (2008).
 - ⁴⁴ N. V. Prokof'ev, B. V. Svistunov, and I. S. Tupitsyn, *JETP* **87**, 310 (1998).
 - ⁴⁵ N. V. Prokof'ev, B. V. Svistunov, and I. S. Tupitsyn, *Physics Letters A* **238**, 253 (1998).
 - ⁴⁶ L. Pollet, K. V. Houcke, and S. M. A. Rombouts, *J. Comp. Phys.* **225**, 2249 (2007).
 - ⁴⁷ H. F. Song, S. Rachel, C. Flindt, I. Klich, N. Laflorencie, and K. Le Hur, *Phys. Rev. B* **85**, 035409 (2012).
 - ⁴⁸ The data obtained from the optimization procedure and the root solver is consistent.
 - ⁴⁹ P. Guillaume, J. Schoukens, and R. Pintelon, *IEEE Transactions on Instrumentation and Measurement* **38**, 1050 (1989).
 - ⁵⁰ Not only the statistical uncertainty of the coefficients but also the mere truncation procedure can lead to imaginary parts in the root finding process.
 - ⁵¹ This is an exact symmetry for $L_A = L/2$ and we checked explicitly that the data for blocks with $\pm\delta N_A$ agrees within the error bars.
 - ⁵² E. G. Dalla Torre, E. Berg, and E. Altman, *Phys. Rev. Lett.* **97**, 260401 (2006).
 - ⁵³ E. Berg, E. G. Dalla Torre, T. Giamarchi, and E. Altman, *Phys. Rev. B* **77**, 245119 (2008).
 - ⁵⁴ L. Amico, G. Mazzarella, S. Pasini, and F. S. Cataliotti, *New Journal of Physics* **12**, 013002 (2010).
 - ⁵⁵ D. Rossini and R. Fazio, *New Journal of Physics* **14**, 065012 (2012).
 - ⁵⁶ G. G. Batrouni, R. T. Scalettar, V. G. Rousseau, and B. Grémaud, (2013), [arXiv:1304.2120](https://arxiv.org/abs/1304.2120) (unpublished).
 - ⁵⁷ F. Pollmann, E. Berg, A. M. Turner, and M. Oshikawa, *Phys. Rev. B* **85**, 075125 (2012).
 - ⁵⁸ A. Läuchli and C. Kollath, *J. Stat. Mech.*, P05018 (2008).
 - ⁵⁹ W. Chen, K. Hida, and B. C. Sanctuary, *Phys. Rev. B* **67**, 104401 (2003).
 - ⁶⁰ This does *not* imply that reducing n_{\max} will yield a better resolution of the entanglement spectrum since the absolute precision due to the truncation of the spectrum will become worse.
 - ⁶¹ Y. Zhang, T. Grover, and A. Vishwanath, *Phys. Rev. Lett.* **107**, 067202 (2011).
 - ⁶² Y. Zhang, T. Grover, and A. Vishwanath, *Phys. Rev. B* **84**, 075128 (2011).
 - ⁶³ Y. Zhang, T. Grover, and A. Vishwanath, *Phys. Rev. B* **85**, 199905 (2012).
 - ⁶⁴ Y. Zhang, T. Grover, A. Turner, M. Oshikawa, and A. Vishwanath, *Phys. Rev. B* **85**, 235151 (2012).
 - ⁶⁵ A. J. Daley, H. Pichler, J. Schachenmayer, and P. Zoller, *Phys. Rev. Lett.* **109**, 020505 (2012).